



HAL
open science

Vibroacoustic responses of a heavy fluid loaded cylindrical shell excited by a turbulent boundary layer

Laurent Maxit, Mahmoud Karimi, Valentin Meyer, Nicole Kessissoglou

► To cite this version:

Laurent Maxit, Mahmoud Karimi, Valentin Meyer, Nicole Kessissoglou. Vibroacoustic responses of a heavy fluid loaded cylindrical shell excited by a turbulent boundary layer. *Journal of Fluids and Structures*, 2020, 92, pp.102758. 10.1016/j.jfluidstructs.2019.102758 . hal-02414405

HAL Id: hal-02414405

<https://hal.science/hal-02414405>

Submitted on 16 Dec 2019

HAL is a multi-disciplinary open access archive for the deposit and dissemination of scientific research documents, whether they are published or not. The documents may come from teaching and research institutions in France or abroad, or from public or private research centers.

L'archive ouverte pluridisciplinaire **HAL**, est destinée au dépôt et à la diffusion de documents scientifiques de niveau recherche, publiés ou non, émanant des établissements d'enseignement et de recherche français ou étrangers, des laboratoires publics ou privés.

Vibroacoustic Responses of a Heavy Fluid Loaded Cylindrical Shell Excited by a Turbulent Boundary Layer

Laurent Maxit¹, Mahmoud Karimi², Valentin Meyer³, Nicole Kessissoglou⁴

1. Univ Lyon, INSA–Lyon, Laboratoire Vibrations-Acoustique (LVA), 25 bis, av. Jean Capelle, F-69621, Villeurbanne Cedex, France

e-mail: laurent.maxit@insa-lyon.fr

2. Centre for Audio, Acoustics and Vibration, University of Technology Sydney, Sydney, Australia

e-mail: mahmoud.karimi@uts.edu.au

3. Naval Group Research, 199 avenue Pierre-Gilles, 83100 Ollioules, France

e-mail: valentin.meyer@naval-group.com

4. School of Mechanical and Manufacturing Engineering, The University of New South Wales, Sydney, NSW 2052, Australia

e-mail: n.kessissoglou@unsw.edu.au

ABSTRACT

A fully coupled structural-acoustic model of a cylindrical shell under external turbulent boundary layer excitation is herein developed. The numerical process requires computation of the wall pressure cross spectral density function as well as sensitivity functions for the fluid-loaded cylindrical shell. A semi-empirical model from literature is used to describe the wall pressure field induced by the turbulent boundary layer in the wavenumber-frequency domain. An analytical expression of the wall pressure field for a flat surface is adapted to describe the wall pressure field for a cylindrical surface. Circumferential sensitivity functions are derived using a wavenumber-point reciprocity principle. Results for the near-field and far-field acoustic pressure spectra are presented. Contributions of individual circumferential modes to the acoustic pressure spectra are examined, showing distinct trends below and above the ring frequency. The proposed

60 method is computationally efficient and provides an effective approach to investigate
61 vibroacoustic responses for maritime platforms.
62
63
64
65

66 **1. Introduction**

67
68 Modelling the vibroacoustic behaviour of structures excited by a random pressure field
69 such as a turbulent boundary layer (TBL) has significant benefit for naval applications.
70 For example, a submerged marine vessel such as an autonomous underwater vehicle or a
71 submarine is excited by pressure fluctuations due to turbulent flow induced by the vessel's
72 movement through the water. Whilst interior and exterior noise from onboard machinery at
73 low speeds and propeller noise at high speeds are dominant noise sources of an underwater
74 vehicle, noise induced by a TBL is important in order to estimate the vessel self-noise. The
75 self-noise radiated by a marine vessel can reduce the signal-to-noise ratio, leading to a
76 reduction in performance of a passive sonar hull-mounted array. As such, understanding
77 the vibroacoustic responses of a submerged vessel under TBL excitation can greatly assist
78 in implementing mitigation strategies to minimize its radiated noise. The motivation of the
79 current work is to develop a computationally efficient model of a fluid-loaded cylindrical
80 shell under TBL excitation and to explore the physical mechanisms contributing to the
81 near and far field structure-borne sound.
82
83
84
85
86
87
88
89
90
91
92
93
94
95
96
97
98

99 Theoretical, numerical and experimental studies have been extensively carried out to
100 predict the vibroacoustic behaviour of plates in air excited by a turbulent flow field (for
101 example, see Ciappi et al., 2014, 2018 and references therein). Strawderman (1969)
102 semi-analytically modelled both an infinite plate and a finite plate under turbulence
103 excitation. The infinite plate model was found to provide a good estimation of the plate
104 vibration power spectra whilst the cross spectral properties of the vibration response were
105 more accurately predicted by the finite plate model. The effect of heavy fluid loading on
106 the two plate models excited by turbulent flow was then examined (Strawderman and
107 Christman, 1971). The propagation speed in the infinite plate as well as resonances of the
108
109
110
111
112
113
114
115
116
117
118

119
120 finite plate were shown to decrease compared with an equivalent plate in air. Davis (1971)
121
122 compared the radiated sound power in air from a thin flexible panel excited by TBL wall
123
124 pressure fluctuations using deterministic and statistical methods. In the deterministic
125
126 method, the radiated sound power was estimated by directly summing over resonant
127
128 modes from a modal analysis. The radiated power was also predicted using Statistical
129
130 Energy Analysis assuming equipartition of energy between plate modes. At frequencies
131
132 above the hydrodynamic coincidence frequency (which occurs when the plate flexural
133
134 wavenumber is equal to the convective wavenumber), results from the two methods were
135
136 shown to converge. Maury et al. (2002a, 2002b) proposed an analytical framework to
137
138 predict the vibroacoustic responses of a panel excited by either a diffuse acoustic field or
139
140 a fully developed turbulent flow. The structural displacement was represented by a
141
142 Green's function representation in the wavenumber domain. An increase in flow velocity
143
144 was observed to more rapidly increase the radiated sound pressure than the turbulent
145
146 pressure. Hambric et al. (2004) used the finite element method (FEM) to examine the
147
148 effect of different edge boundary conditions on the response of a flat plate under TBL
149
150 excitation. They also proposed an approximate TBL model representing only the surface
151
152 interaction, which was shown to work well for plates with clamped boundary conditions
153
154 and at low wavenumber. De Rosa et al. (2008) analytically and numerically studied the
155
156 structural response of a plate excited by a TBL using the modal expansion method and
157
158 FEM. A scaling procedure was applied to both methods, leading to a significant reduction
159
160 in simulation run time. Errico et al. (2019) proposed a numerical approach to estimate the
161
162 sound transmission loss of complex flat, curved and cylindrical periodic structures, under
163
164 acoustic or aerodynamic loads. The structural domain was modelled using the wave finite
165
166 element method. The fluid-structure interaction was simulated in analogy to the acoustic
167
168 wave excitation, discriminating among the different forcing models, using weighted
169
170 wavenumber integration. For planar structures, the finite-size effects were taken into
171
172
173
174
175
176
177

178
179 account using either the baffled window equivalence or asymptotic formulations. The
180 approach was validated against experimental results. Ciappi et al. (2009) numerically and
181 experimentally studied the response of a fluid-loaded plate under TBL excitation. The
182 Corcos and Chase models were employed to predict the plate response. The Chase model
183 was shown to provide good agreement between numerical and experimental results for the
184 structure-borne acoustic responses. An approach based on sensitivity functions and
185 reciprocity principles was employed by Marchetto et al. (2017, 2018) to model panels
186 under diffuse acoustic field and TBL excitation. The vibroacoustic responses at any
187 location either on the panel or in the acoustic medium was shown to depend on two
188 quantities in the wavenumber domain; namely, the wall-pressure cross spectral density
189 function of the excitation and the sensitivity function at that location. Mazzoni (2003)
190 presented an analytical model based on wavenumber integration to approximate the
191 vibroacoustic response of an elastic water-loaded plate excited by a TBL at low Mach
192 number. Greater sensitivity of the plate modes in the subconvective region of the power
193 spectrum of the turbulent excitation was observed.

200
201
202
203
204
205
206
207
208
209
210
211 The vibroacoustic responses of curved and composite panels under TBL excitation have
212 also received attention. A deterministic approach combining modal expansion and
213 receptance methods was developed by Liu (2008) to predict the radiated sound from
214 aircraft panels subject to TBL excitation. The response of aerospace composite plates
215 under turbulence induced vibration was numerically and experimentally investigated by
216 Ciappi et al. (2016). They showed that at high Mach number, the aeroelastic effect on the
217 panel response cannot be neglected, especially when composite materials are considered.

220
221
222
223
224
225
226 One of the earliest works on TBL excitation of cylindrical shells was presented by
227 Norton and Bull (1984), to experimentally investigate the vibroacoustic responses of a
228 thin cylindrical pipe excited by turbulent internal flow. At low frequencies where only
229 acoustic plane waves can propagate in the pipe, peristaltic motion and resonant modes of
230
231
232
233
234
235
236

237
238 the pipe wall were shown to contribute to the structural response. At higher frequencies,
239
240 acoustic coincidence effects led to strong excitation of supersonic pipe modes, resulting in
241
242 increasing pipe wall vibration and external radiation. Durant et al. (2000) numerically
243
244 computed the structural and acoustic responses of a thin cylindrical pipe excited by
245
246 turbulent internal flow using a boundary integral formulation. The wall pressure excitation
247
248 was described by a Corcos model with the input parameters obtained from measurement of
249
250 the cross spectral density of the wall pressure fluctuations. Recently, Li et al. (2017)
251
252 studied random vibration analysis of an axially compressed cylindrical shell in air excited
253
254 by an external TBL. The governing differential equations of the axially compressed
255
256 cylindrical shell were derived and the eigenproblem was formed using the separation of
257
258 variables technique. The cross spectrum density of the TBL was expanded as a Fourier
259
260 series. Results for the shell responses were compared with those obtained using the modal
261
262 decomposition method, showing good agreement.
263
264

265
266 Various studies have also been conducted to assess the acoustic performance of a
267
268 double-walled cylindrical shell excited by external TBL pressure fluctuations. Tang et al.
269
270 (1996) developed an analytical model for sound transmission in concentric cylindrical
271
272 sandwich shells under TBL excitation of the outer shell surface. It was shown that the
273
274 interior pressure was strongly affected by resonant modes above the hydrodynamic and
275
276 acoustic coincidence frequencies at which noise can be transmitted efficiently. Zhou et al.
277
278 (2015) analytically studied the effect of poroelastic material in the shell core on sound
279
280 transmission in concentric cylindrical shells under external TBL excitation. The shell
281
282 displacements and acoustic pressure in the interior, exterior and annular fluid domains
283
284 were expressed by the modal expansion method. They showed that the shell responses due
285
286 to TBL excitation formulated by the Corcos and Efimtsov models were similar at higher
287
288 frequencies. In a similar study, Zhang et al. (2018) investigated the effect of
289
290 microperforation at the inner wall on sound transmission in a double walled cylindrical
291
292
293
294
295

296
297 shell under external TBL excitation.
298

299 In this paper, a numerical approach is presented to predict the vibroacoustic responses
300 of a cylindrical shell immersed in a heavy fluid and excited by a TBL. The approach is
301 computationally efficient, allowing the influence of individual circumferential modes on
302 the structural and acoustic responses of the shell to be examined in detail. In the first step,
303 the wall pressure field induced by the TBL in the wavenumber-frequency domain is
304 described using a semi-empirical TBL model from literature. In the wavenumber domain,
305 circumferential sensitivity functions which correspond to the structure-borne sound
306 pressure from the cylindrical shell under unit wall plane waves are derived using a
307 reciprocity relation between the acoustic pressure at a spatial location in the fluid and a
308 radial force applied to the shell. The auto spectral density of the pressure in the acoustic
309 near field and far field is then obtained. For insight into the physical mechanisms
310 contributing to the near-field and far-field acoustic spectra, results are presented in terms
311 of individual contributions of circumferential modes, in both the low and high frequency
312 ranges below and above the ring frequency, and for increasing radial distance from the
313 shell. The proposed method provides an effective tool to investigate noise and vibration of
314 underwater vehicles.
315
316
317
318
319
320
321
322
323
324
325
326
327
328
329
330
331
332

333 **2. Methodology**

334 **2.1 Cylindrical shell under TBL excitation**

335 Let us consider an infinitely long thin cylindrical shell immersed in a fluid as shown in
336 Fig. 1. A fully developed, stationary and homogeneous TBL excites the shell. It is assumed
337 that the boundary layer is weakly coupled with the shell vibration and propagation of
338 acoustic waves in the fluid is not affected by the flow.
339
340
341
342
343
344
345
346
347
348
349
350
351
352
353
354

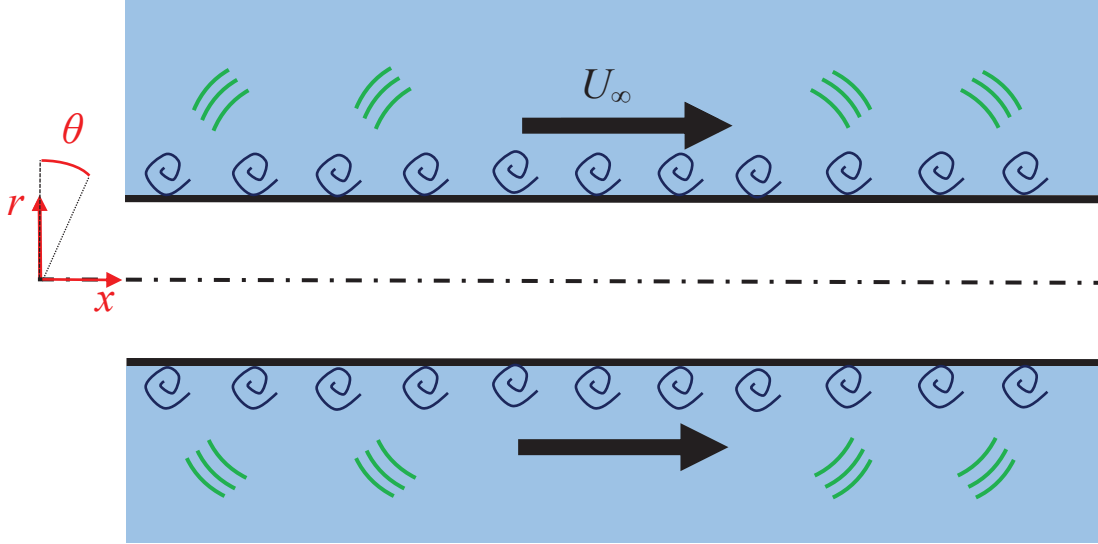


Figure 1. Schematic diagram of an infinitely long cylindrical shell immersed in heavy fluid and excited by a turbulent boundary layer.

The auto spectral density (ASD) of the radiated pressure from the cylindrical shell excited by the TBL is given by (Maury et al. 2002a)

$$S_{pp}(x, \theta, r, \omega) = \int_{-\infty}^{\infty} \int_{-\infty}^{\infty} \int_0^{2\pi} \int_0^{2\pi} |H_{p/F}(x, \theta, r, x_1, \theta_1, \omega)|^2 S_{pp}^{\text{TBL}}(x_2 - x_1, \theta_2 - \theta_1, \omega) R^2 d\theta_1 d\theta_2 dx_1 dx_2 \quad (1)$$

where $H_{p/F}(x, \theta, r, x_1, \theta_1, \omega)$ is the frequency response function (FRF) of the radiated pressure at point M in the fluid with coordinate (x, θ, r) for radial point force excitation of the shell at M_1 . $S_{pp}^{\text{TBL}}(x_2 - x_1, \theta_2 - \theta_1, \omega)$ is the cross spectral density (CSD) function of the wall pressure field between two points on the shell surface and is formulated in the following section.

2.2 Wall pressure field

The wall pressure field (WPF) induced by the TBL can be described by one of several semi-empirical TBL models proposed in the literature (for example, see Corcos 1963, Chase 1987, Goody 2004). Whilst these models have been established for planar structures such as a flat plate, they are assumed to accurately describe the WPF at the surface of a

414 shell for low curvature (Lueptow 1988). For planar structures, the CSD function of the
 415 WPF in the wavenumber space, denoted by $\varphi_{pp}(k_x, k_y, \omega)$, is related to the CSD function
 416 of the WPF in the physical space, $S_{pp}^{\text{TBL}}(x, y, \omega)$, as follows
 417
 418
 419
 420
 421

$$422 \varphi_{pp}(k_x, k_y, \omega) = \int_{-\infty}^{\infty} \int_{-\infty}^{\infty} S_{pp}^{\text{TBL}}(x, y, \omega) e^{-ik_x x} e^{-ik_y y} dx dy, \quad (2)$$

$$423 S_{pp}^{\text{TBL}}(x, y, \omega) = \frac{1}{(2\pi)^2} \int_{-\infty}^{\infty} \int_{-\infty}^{\infty} \varphi_{pp}(k_x, k_y, \omega) e^{ik_x x} e^{ik_y y} dk_x dk_y, \quad (3)$$

424 where ω is the angular frequency, and k_x, k_y are wavenumber components in the x - and
 425 y -directions, respectively. The x -axis represents the streamwise direction and the y -axis
 426 represents the spanwise direction.
 427

428 For the cylindrical shell considered in this work, the spanwise direction y
 429 corresponds to the shell circumferential direction θ and the WPF is circumferentially
 430 periodic. The wavenumber-frequency domain of the cylindrical shell is denoted by (k_x, n) ,
 431 where n is the circumferential mode number. The CSD function of the WPF in the
 432 wavenumber-frequency domain for a cylindrical shell, denoted by $\phi_{pp}(k_x, n, \omega)$ is related
 433 to $\varphi_{pp}(k_x, k_y, \omega)$ for a planar structure by
 434
 435
 436
 437
 438
 439
 440
 441
 442
 443
 444
 445
 446
 447
 448
 449
 450
 451

$$452 \phi_{pp}(k_x, n, \omega) = \frac{1}{2\pi R} \varphi_{pp}(k_x, k_y, \omega), \quad (4)$$

453 where R is the shell radius. The CSD function of the WPF for the cylindrical shell in the
 454 spatial domain is then obtained as
 455
 456
 457
 458
 459

$$460 S_{pp}^{\text{TBL}}(x, \theta, \omega) = \frac{1}{2\pi} \sum_{n=-\infty}^{+\infty} \left\{ \int_{-\infty}^{+\infty} \phi_{pp}(k_x, n, \omega) e^{ik_x x} dk_x \right\} e^{in\theta}. \quad (5)$$

461 2.3 Circumferential sensitivity function

462 Substituting Eq. (5) into Eq. (1), the ASD function of the radiated pressure can be
 463 rewritten in the following form:
 464
 465
 466
 467
 468
 469
 470
 471
 472

$$S_{pp}(x, \theta, r, \omega) = 2\pi \sum_{n=-\infty}^{\infty} \int_{-\infty}^{\infty} |\tilde{H}_p(x, \theta, r, k_x, n, \omega)|^2 \phi_{pp}(k_x, n, \omega) dk_x, \quad (6)$$

where

$$\tilde{H}_p(x, \theta, r, k_x, n, \omega) = \frac{1}{2\pi} \int_{-\infty}^{\infty} \int_0^{2\pi} H_{p/F}(x, \theta, r, x_1, \theta_1, \omega) e^{-ik_x x_1} e^{-in\theta_1} R d\theta_1 dx_1. \quad (7)$$

$\tilde{H}_p(x, \theta, r, k_x, n, \omega)$ corresponds to the radiated pressure at point M when the shell is excited by a unit WPF given by $p(x, \theta) = e^{-i(k_x x + n\theta)}$, and is termed the circumferential sensitivity function. The circumferential sensitivity function can be derived using a wavenumber-point reciprocity technique (Maxit and Denis 2013). The Lyamshev reciprocity principle as illustrated in Figure 2 states that the ratio of the radiated pressure p at point M to a radial point force F located at point M_1 is equal to the ratio of the radial velocity v at point M_1 to the volume velocity Q_v at point M , that is,

$$H_{p/F}(x, \theta, r, x_1, \theta_1, \omega) = H_{v/Q_v}(x_1, \theta_1, x, \theta, r, \omega). \quad (8)$$

Substituting Eq. (8) into Eq. (7) yields

$$\tilde{H}_p(x, \theta, r, k_x, n, \omega) = \frac{1}{2\pi} \int_{-\infty}^{\infty} \int_0^{2\pi} H_{v/Q_v}(x_1, \theta_1, x, \theta, r, \omega) e^{-ik_x x_1} e^{-in\theta_1} R d\theta_1 dx_1. \quad (9)$$

The circumferential sensitivity function can now be interpreted as the product of the radius R with the Fourier transform of the shell radial velocity along the axial direction as well as a Fourier series decomposition in the circumferential direction, for the shell excited by an acoustic monopole located at point M with coordinate (x, θ, r) and strength of unit volume velocity. Calculation of the circumferential sensitivity function requires the spectral radial velocity of the fluid-loaded cylindrical shell which is derived in the proceeding section.

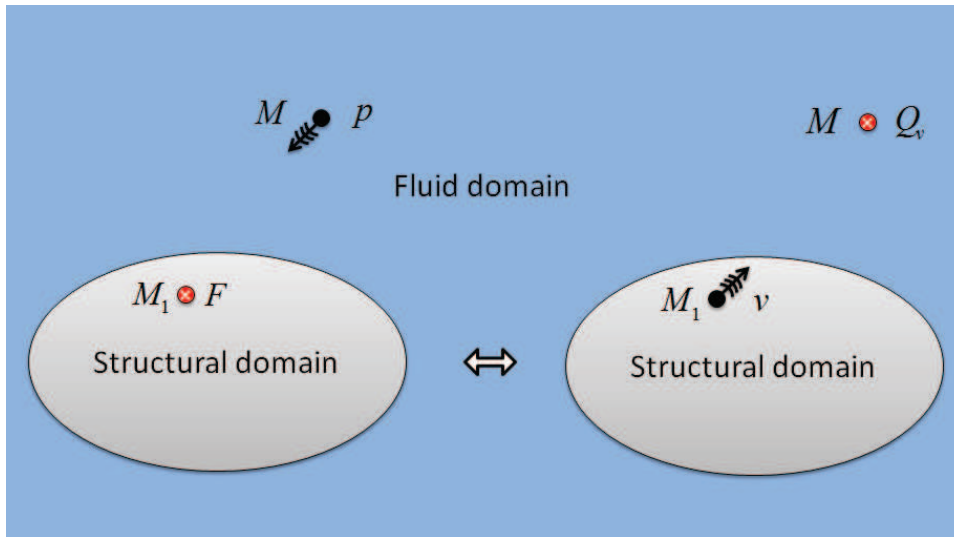


Figure 2. Illustration of the Lyamshev reciprocity principle between structural and fluid domains.

2.4 Fluid-loaded cylindrical shell

The cylindrical shell has radius R , thickness h , Young's modulus E , density ρ_s and Poisson's ratio ν . U , V , and W are respectively the longitudinal, tangential and radial displacements of the shell. The shell is immersed in an infinite fluid domain of density ρ_f and speed of sound c_f . The system is excited by a monopole source at point M with coordinate (x, θ, r) . The blocked wall pressure at $r = R$, corresponding to the induced WPF by the monopole when the shell is considered as rigid, is denoted by p_b . The structure-borne radiated wall pressure in the exterior acoustic domain is denoted by p_r .

Assuming the following time harmonic dependency $e^{i\omega t}$, the Flügge equations of motion of the cylindrical shell are given by (Leissa 1973, Karczub 2006)

$$\mathcal{L}(x, \theta) \begin{bmatrix} U(x, \theta) \\ V(x, \theta) \\ W(x, \theta) \end{bmatrix} = \gamma \left(\begin{bmatrix} 0 \\ 0 \\ p_b(x, \theta) \end{bmatrix} + \begin{bmatrix} 0 \\ 0 \\ -p_r(x, \theta) \end{bmatrix} \right), \quad (10)$$

where $\gamma = \frac{(1-\nu^2)R^2}{Eh}$ and the elements of the spectral Flügge operator $\mathcal{L}(x, \theta)$ are

591 listed in Appendix A. Applying both a Fourier series decomposition along the
 592 circumferential direction and a Fourier transform along the axial direction to Eq. (10)
 593 yields the shell equations of motion in the wavenumber domain as follows
 594
 595
 596
 597

$$598 \quad \tilde{\mathcal{L}}(k_x, n) \begin{bmatrix} \tilde{U}(k_x, n) \\ \tilde{V}(k_x, n) \\ \tilde{W}(k_x, n) \end{bmatrix} = \gamma \left(\begin{bmatrix} 0 \\ 0 \\ \tilde{p}_b(k_x, n) \end{bmatrix} + \begin{bmatrix} 0 \\ 0 \\ -\tilde{p}_r(k_x, n) \end{bmatrix} \right). \quad (11)$$

600 The elements of spectral Flügge matrix $\tilde{\mathcal{L}}(k_x, n)$ in the wavenumber domain are listed in
 601 Appendix B.
 602
 603
 604

605 Considering a monopole of unit volume velocity at point M in the acoustic domain, the
 606 spectral blocked pressure at the external surface of the cylinder can be derived in a similar
 607 manner described by James (1982) as follows:
 608
 609

$$610 \quad \tilde{p}_b(k_x, n) = \frac{i\omega\rho_f}{2\pi k_r R} \frac{H_n^{(2)}(k_r r)}{H_n^{(2)'}(k_r R)} e^{-i(n\theta + k_x x)} \quad (12)$$

611 where $H_n^{(2)}$ is the Hankel function of the second kind of order n , $()'$ denotes the
 612 derivative with respect to the argument, and k_r is given by
 613
 614
 615

$$616 \quad k_r = \begin{cases} \sqrt{k_f^2 - k_x^2} & \text{if } |k_x| \leq k_f, \\ -i\sqrt{k_x^2 - k_f^2} & \text{otherwise.} \end{cases} \quad (13)$$

617 In the acoustic domain, the radiated pressure from the vibrating shell satisfies the
 618 homogeneous Helmholtz equation (Junger and Feit 1986)
 619
 620
 621

$$622 \quad \Delta p_r(x, \theta, r) + k_f^2 p_r(x, \theta, r) = 0, \quad (14)$$

623 where Δ is the Laplacian operator in the cylindrical coordinate system. The kinematic
 624 condition at the cylindrical interface between the shell and fluid medium is given by
 625
 626
 627
 628
 629
 630
 631
 632
 633
 634
 635
 636
 637
 638
 639
 640
 641
 642 (Junger and Feit 1986)

$$643 \quad \frac{\partial p_r}{\partial r}(x, \theta, R) = \rho_f \omega^2 W(x, \theta). \quad (15)$$

650
651 Applying Fourier transforms to Eqs. (14) and (15), the spectral radiated wall pressure
652
653 denoted by \tilde{p}_r can be expressed in terms of the spectral radial displacement of the shell
654
655 denoted by \tilde{W} as well as the spectral fluid impedance, \tilde{Z}_f , as follows
656
657

$$658 \quad \tilde{p}_r(k_x, n) = \tilde{Z}_f(k_x, n) \tilde{W}(k_x, n), \quad (16)$$

$$659 \quad \tilde{Z}_f(k_x, n) = \frac{\rho_f \omega^2 H_n^{(2)}(k_r R)}{k_r H_n^{(2)'}(k_r R)}. \quad (17)$$

660
661
662 Substituting Eqs. (16) and (17) into Eq. (11) and inverting the matrix system yields the
663
664 following expression for the spectral radial displacement:
665
666

$$667 \quad \tilde{W}(k_x, n) = \frac{\gamma \tilde{p}_b(k_x, n) \left(\tilde{Z}_{UU}(k_x, n) \tilde{Z}_{VV}(k_x, n) - (\tilde{Z}_{UV}(k_x, n))^2 \right)}{\Gamma(k_x, n)}, \quad (18)$$

668
669 where

$$670 \quad \Gamma(k_x, n) = \left| \tilde{\mathcal{L}}_{FL}(k_x, n) \right| = \tilde{Z}_{UW} \left(\tilde{Z}_{UV} \tilde{Z}_{VW} - \tilde{Z}_{UV} \tilde{Z}_{VV} \right) + \tilde{Z}_{VW} \left(\tilde{Z}_{UW} \tilde{Z}_{UV} - \tilde{Z}_{VW} \tilde{Z}_{UU} \right) + \quad (19)$$

$$671 \quad \left(\tilde{Z}_{WW} + \gamma \tilde{Z}_f \right) \left(\tilde{Z}_{UU} \tilde{Z}_{VV} - \tilde{Z}_{UV}^2 \right)$$

672
673
674 The spectral radial velocity of the fluid loaded cylindrical shell is $i\omega \tilde{W}(k_x, n)$. Using Eqs.
675
676 (12) and (18), the circumferential sensitivity function becomes

$$677 \quad \tilde{H}_p(x, \theta, r, k_x, n, \omega) = \frac{i\omega \rho_f \gamma e^{-i(n\theta + k_x x)} H_n^{(2)}(k_r r_s)}{2\pi k_r H_n^{(2)'}(k_r R)} \frac{\left(\tilde{Z}_{UU}(k_x, n) \tilde{Z}_{VV}(k_x, n) - (\tilde{Z}_{UV}(k_x, n))^2 \right)}{\Gamma(k_x, n)} \quad (20)$$

678
679 Substituting the circumferential sensitivity function given by Eq. (20) and the CSD
680
681 function of the WPF given by Eq. (4) into Eq. (6) yields the ASD of the sound pressure
682
683 from the cylindrical shell under TBL excitation.
684
685

686 2.5 Wavenumber domain truncation

687
688 The integral and summation of the ASD in Eq. (6) are with respect to infinite domains. In
689
690 practice, these domains are truncated. [The lowest frequency considered in this work is greater](#)
691
692
693
694
695
696
697
698
699
700
701
702
703
704
705
706
707
708

709
710
711 than the hydrodynamic coincidence frequency, which corresponds to the case when the
712
713 flexural wavenumber of a plate denoted by k_p with the same thickness and material
714
715 properties of the cylindrical shell equals the convective wavenumber given by $k_c = \omega/U_c$,
716
717 where U_c is the convective velocity. The contributions of convective peaks to the acoustic
718
719 pressure are then generally negligible (Hambric et al. 2004, Maxit 2016). As such, in the
720
721 definition of the cut-off axial wavenumber, the convective wavenumber was not included.
722
723 One can then define a cut-off axial wavenumber $k_{x,co}$ from the characteristics of the shell and
724
725 fluid as follows

$$732 \quad k_{x,co} = \kappa_x \max(k_p, k_f), \quad (21)$$

733
734 where $k_f = \omega/c_f$ is the acoustic wavenumber and κ_x is a margin coefficient (typically
735
736 $\kappa_x = 2$) (Maxit and Ginoux 2010). Similarly, the cut-off circumferential order N_{co} can
737
738 be defined by

$$741 \quad N_{co} = \text{int} \left[\kappa_N R \max(k_p, k_f) \right] + 1, \quad (22)$$

742
743 where κ_N is a second margin coefficient (typically $\kappa_N = 1.5$) (Maxit and Ginoux 2010).
744
745

746
747 Applying the cut-off axial wavenumber and the cut-off circumferential order, the ASD of
748
749 the acoustic pressure given by Eq. (6) now becomes

$$752 \quad S_{pp}(x, \theta, r, \omega) \approx 2\pi \sum_{n=-N_{co}}^{n=N_{co}} \int_{-k_{x,co}}^{k_{x,co}} \left| \tilde{H}_p(x, \theta, r, k_x, n, \omega) \right|^2 \phi_{pp}(k_x, n, \omega) dk_x, \quad (23)$$

753
754 where the integral may be estimated numerically using the rectangular rule. To study the
755
756 individual contributions of the circumferential modes to the ASD, Eq. (23) can be written

757
758 as $S_{pp}(x, \theta, r, \omega) \approx \sum_{n=0}^{N_{co}} C_n$ with C_n the contribution of the n^{th} mode given by
759
760
761
762
763
764
765
766
767

$$C_n = 2\pi\varepsilon_n \int_{-k_{x,co}}^{k_{x,co}} \left| \tilde{H}_p(x, \theta, r, k_x, n, \omega) \right|^2 \phi_{pp}(k_x, n, \omega) dk_x, \quad (24)$$

$$\text{where } \varepsilon_n = \begin{cases} 1 & \text{for } n = 0 \\ 2 & \text{for } n \in [1, N_{co}] \end{cases}$$

3. Numerical results

An infinite cylindrical shell submerged in water with a radius of $R=5$ m and thickness of $h=0.05$ m is studied here. The shell is made of steel with density $\rho_s = 7800$ kg/m³, Young's modulus $E = 2.1 \times 10^{11}$ Pa, Poisson's ratio $\nu = 0.3$, and structural loss factor $\eta = 0.02$. The density and speed of sound in the water are $\rho_f = 1000$ kg/m³ and $c_f = 1500$ m/s, respectively. A freestream velocity of $U_\infty = 6$ m/s was assumed, which forms a homogeneous fully developed turbulent boundary layer on the surface of the shell. A friction velocity of $v_\tau = 1$ m/s and boundary layer thickness of $\delta = 0.15$ m was used in the numerical calculations. The Chase TBL model, valid for $\omega\delta/U_\infty \gg 1$, was employed to model the CSD function of the wall pressure field. The expression for the CSD of the Chase model can be found in Appendix C. Using the aforementioned TBL parameters, the Chase model can be confidently implemented for frequencies greater than 10 Hz. As the original spectrum given by the Chase model is a two-sided angular frequency spectrum, it was multiplied by 4π to convert it to a one-sided frequency spectrum. In addition, due to the difference between the Fourier conventions used in Chase (1987) and the current work, the wall pressure spectrum was multiplied by $(2\pi)^3$ to have the same Fourier convention.

The vibroacoustic responses of the shell were calculated for a frequency range between 10 Hz to 1000 Hz. Three distinct frequencies relevant to the current analysis correspond to the hydrodynamic coincidence frequency, the ring frequency and the acoustic coincidence frequency, corresponding to the frequency at which the equivalent plate flexural wavenumber is equal to the acoustic wavenumber. For the parameters chosen here, the

827 hydrodynamic coincidence frequency is 0.036 Hz and the critical frequency is 4561 Hz.
828
829
830 As such, only the ring frequency of the cylindrical shell, occurring at 173 Hz, lies in the
831
832 frequency range of interest. At the ring frequency, the shell resonates as a ring due to the
833
834 fact that longitudinal waves travel in the shell with a wavelength equal to the shell
835
836 circumference. Below the ring frequency, the effect of the shell curvature is important and
837
838 most of the shell vibrational energy is in stretching. Above the ring frequency, the shell
839
840 vibrates in a similar way to a flat plate and most of the energy is in bending (Fahy and
841
842 Gardonio, 2007).
843
844

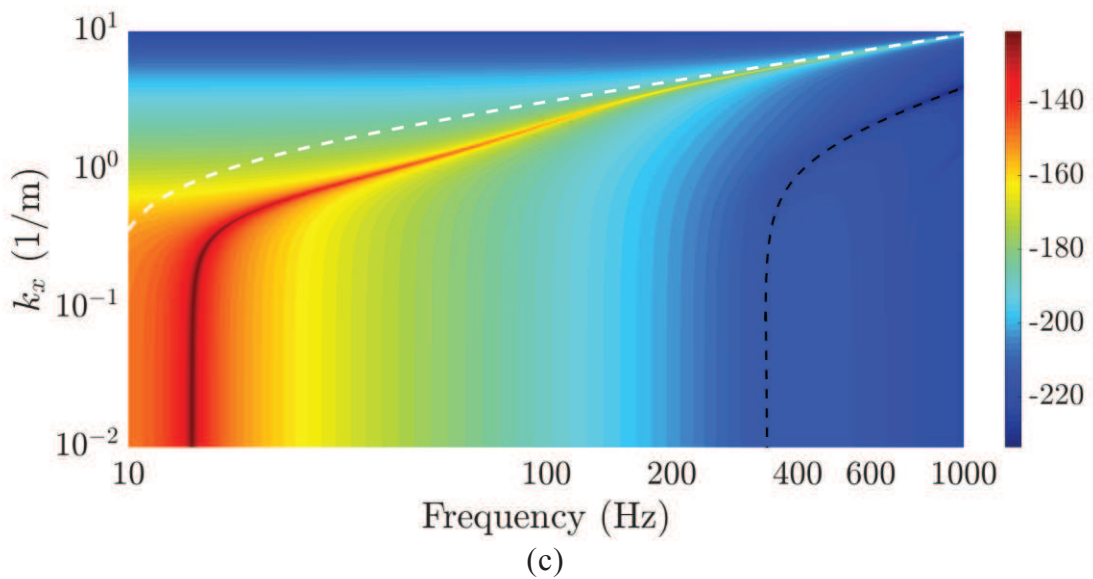
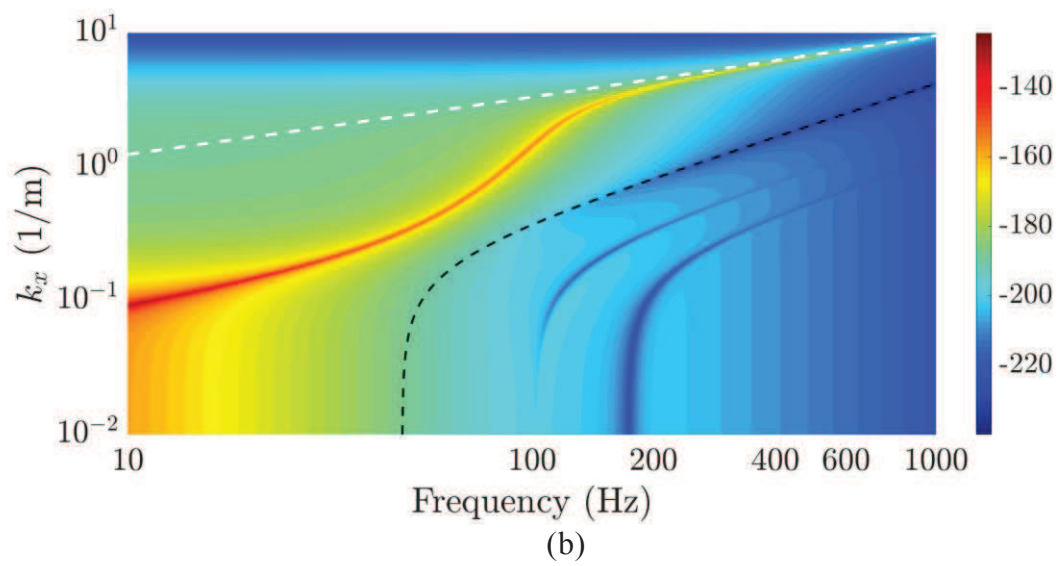
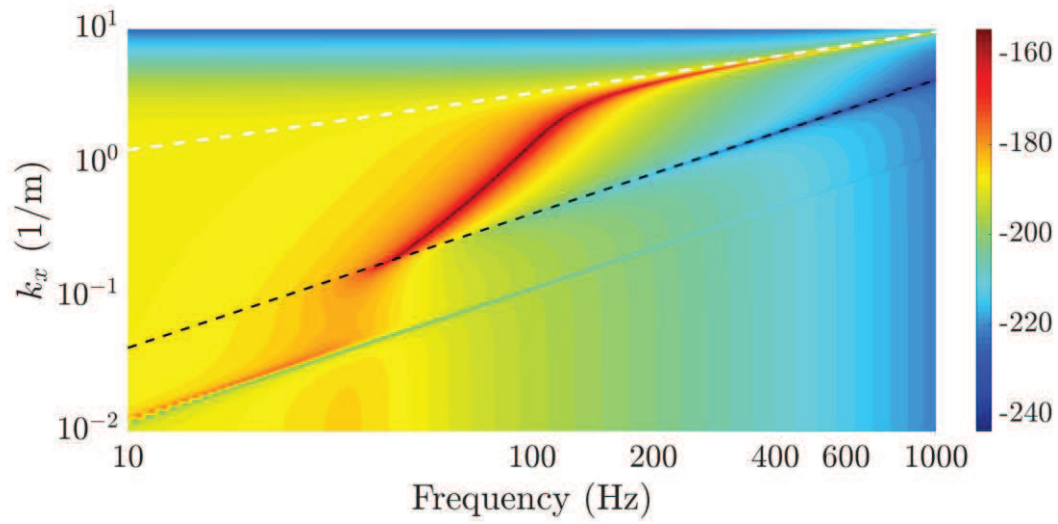
845 3.1 Spectral displacement of the fluid loaded shell

846
847
848
849 The vibratory response of the fluid loaded shell in the wavenumber domain under point
850
851 force excitation is initially examined. The radial point force $p_F(x, \theta) = \delta(x)\delta(\theta)$ is
852
853 applied at $(x, \theta) = (0, 0)$, thereby exciting all axial wavenumber components and
854
855 circumferential modes with the same magnitude. The Fourier transform of the pressure
856
857 distribution due to the radial point force is $\tilde{p}_F(k_x, n) = \frac{1}{2\pi}$. The spectral displacement of
858
859 the shell is then given by
860
861
862
863

$$864 \tilde{W}_F(k_x, n) = \frac{\tilde{p}_F(k_x, n) \gamma \left(\tilde{Z}_{UU}(k_x, n) \tilde{Z}_{VV}(k_x, n) - \left(\tilde{Z}_{UV}(k_x, n) \right)^2 \right)}{\Gamma(k_x, n)} \quad (25)$$

865
866
867
868
869 which differs from Eq. (18) with the term \tilde{p}_F instead of \tilde{p}_b . Figure 3 presents the
870
871 spectral shell displacement at three discrete circumferential modes corresponding to $n=0$,
872
873 $n=1$ and $n=7$. In each figure, the acoustic wavenumber k_f , denoted by a black dashed line,
874
875 as well as the flexural wavenumber of an equivalent fluid loaded plate denoted by a white
876
877 dashed line, are also shown. The flexural wavenumber of a fluid loaded plate was
878
879 calculated using $k_{p,FL} = \left(k_p^4 + \omega^2 \rho_f / (D \sqrt{k_p^2 - k_f^2}) \right)^{1/4}$, where $k_p = (\omega^2 \rho_s h / D)^{1/4}$ is the
880
881
882
883
884
885

886
887 flexural wavenumber of the in vacuo plate and the second term in brackets is the added
888 mass to take into account the fluid loading effects. Figure 3(a) shows that at low
889 frequencies, the axisymmetric $n=0$ mode is a subsonic wave (with axial wavenumber
890 components greater than the acoustic wavenumber), whereby the axial wavenumber is
891 exponentially close to the acoustic wavenumber. As frequency increases, the wavenumber
892 increases and asymptotes to that of the plate flexural wavenumber above the ring
893 frequency. This finding has been previously reported by Photiadis (1990). For the $n=1$
894 bending mode in Figure 3(b), the strong effect of the shell curvature at low frequencies can
895 be observed. Similar to the $n=0$ mode, the axial wavenumber components of the $n=1$
896 mode are subsonic and above the ring frequency, asymptote to the plate flexural
897 wavenumber. The cut-on frequencies of the quasi-compressional and shear waves can also
898 be observed at around 100 Hz and 170 Hz, respectively. The first circumferential mode to
899 cut on in the frequency range from 10 Hz to 1 kHz corresponds to the $n=7$ mode at a cut-on
900 frequency of 14 Hz (Figure 3(c)). Here it is observed that the spectral displacement is close
901 the plate flexural wavenumber. Similar findings for subsonic waves of a fluid-loaded
902 cylindrical shell to those presented here have been previously observed in the dispersion
903 graphs reported by Scott (1988).
904
905
906
907
908
909
910
911
912
913
914
915
916
917
918
919
920
921
922
923
924
925
926
927
928
929
930
931
932
933
934
935
936
937
938
939
940
941
942
943
944



997
998
999
1000
1001
1002
1003

Figure 3. Spectral displacement of the shell under radial point force excitation for (a) $n=0$, (b) $n=1$ and (c) $n=7$. The black dashed line denotes the acoustic wavenumber and the white dashed line corresponds to the flexural wavenumber of an equivalent fluid loaded plate.

3.2 Near field acoustic spectra

Figure 4 presents the ASD function of the acoustic pressure in the near field as a function of frequency. Contributions by individual circumferential modes to the acoustic spectrum are also shown. The $n=0$ and $n=1$ modes do not cut on at specific frequencies in the frequency range of interest, as shown previously in Figures 3(a) and 3(b), respectively. Below the ring frequency, the subsonic waves associated with these modes have negligible contribution to the near-field acoustic response. The distinct peaks in the acoustic spectra correspond to $n \geq 2$ shell circumferential modes that cut on at specific frequencies. The first peak in Figure 4 corresponds to the $n=7$ mode at a cut on frequency of 14 Hz, as shown previously in Figure 3(c) (whereby the $n=2-6$ modes cut on below 10 Hz). Below their respective cut-on frequency, the $n \geq 2$ modes have very little contribution to the near-field acoustic spectrum. In contrast, at respective cut on frequencies that occur below the ring frequency, these modes have a significant effect on the near-field acoustic response. Above the ring frequency, all modes have similar contribution to the total acoustic spectrum. The $n=0$ mode asymptotes to a lower value by a constant amount of around 3 dB, associated with the fact that C_n in Eq. (24) is defined as the sum of the contribution corresponding to $[-n, n]$ for all $n \geq 1$ modes and as such, is twice the value of C_0 .

Circumferential sensitivity functions for the cylindrical shell in the near field ($z=0.1$ m) are presented in Figure 5 at three distinct frequencies, corresponding to 10 Hz, 100 Hz and 1000 Hz. Two semi-ellipse curves are also depicted in Figure 5 whereby similar to Figure 3, the black dashed line is associated with the acoustic wavenumber represented by

$\{k_x, R\sqrt{k_f^2 - k_x^2}\}$ where $k_x \in [-k_f, k_f]$, and similarly, the white dashed line is associated

with the flexural wavenumber of an equivalent fluid-loaded plate represented by

$\{k_x, R\sqrt{k_{p,FL}^2 - k_x^2}\}$ where $k_x \in [-k_{p,FL}, k_{p,FL}]$. Figure 5 shows that in the acoustic near

field, the maxima of the sensitivity function are located on the semi-ellipse that corresponds to flexural vibration of an equivalent fluid loaded plate. These values are essentially the roots of the characteristic equation given by Eq. (19). Figure 5(a) shows that a maximum of 6 circumferential modes contribute to the acoustic spectrum at 10 Hz (the $n=7$ mode cuts on at 14 Hz as shown previously in Figure 4). At 100 Hz in Figure 5(b), it can be observed that around 15 circumferential modes contribute to the acoustic pressure whilst at 1000 Hz (Figure 5(c)), around 50 circumferential modes contribute to the pressure spectrum. The subsonic waves associated with the wavenumber region outside the acoustic semi-ellipse correspond to evanescent waves that propagate close to the cylinder and only contribute to the near field pressure spectrum. These results are consistent with the cut on modes discussed previously in Figure 4. Figure 5(c) also shows that as frequency increases, the contribution by C_n for the lowest order circumferential modes increases attributed to the acoustic filtering effect, which will be discussed subsequently.

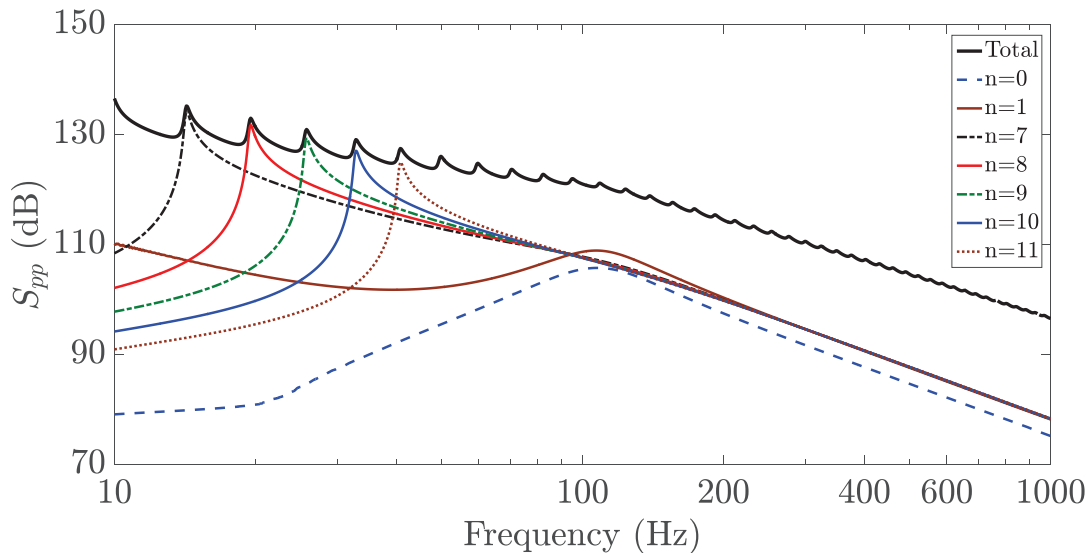


Figure 4. Auto spectral density of the acoustic pressure at $z=0.1$ m (dB ref. $1 \mu\text{Pa}/\sqrt{\text{Hz}}$).

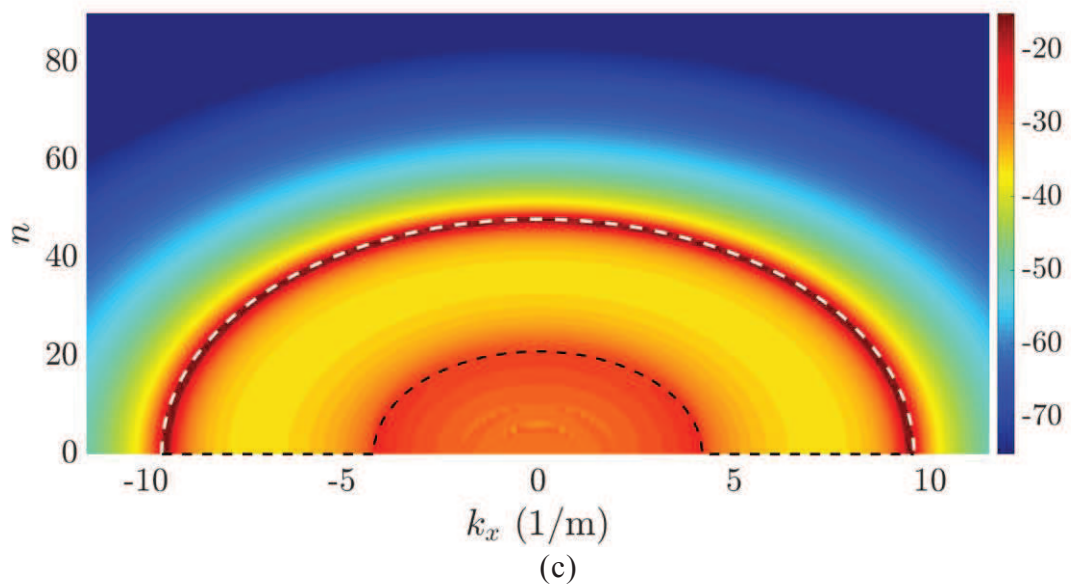
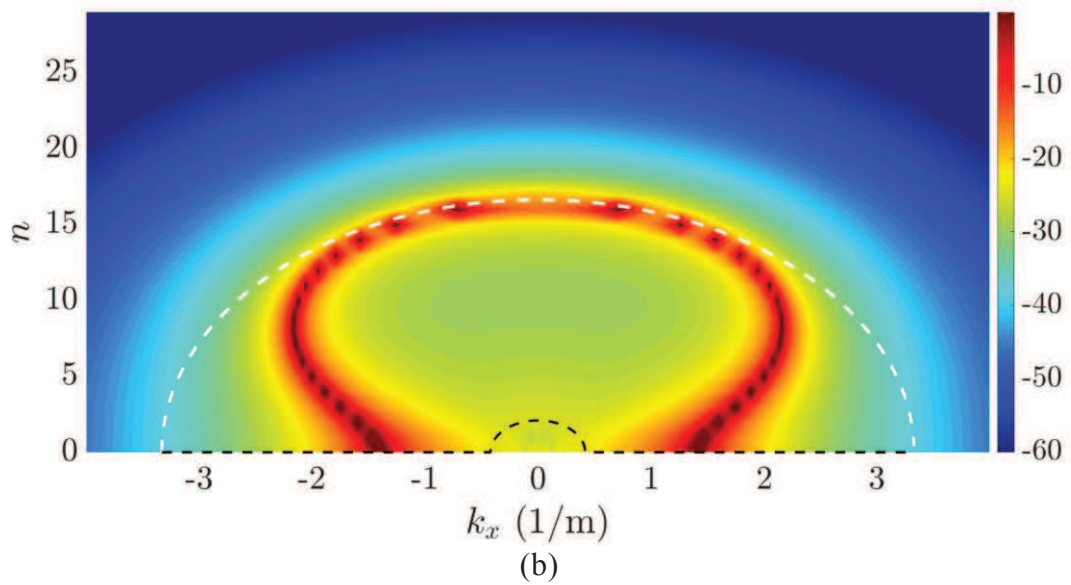
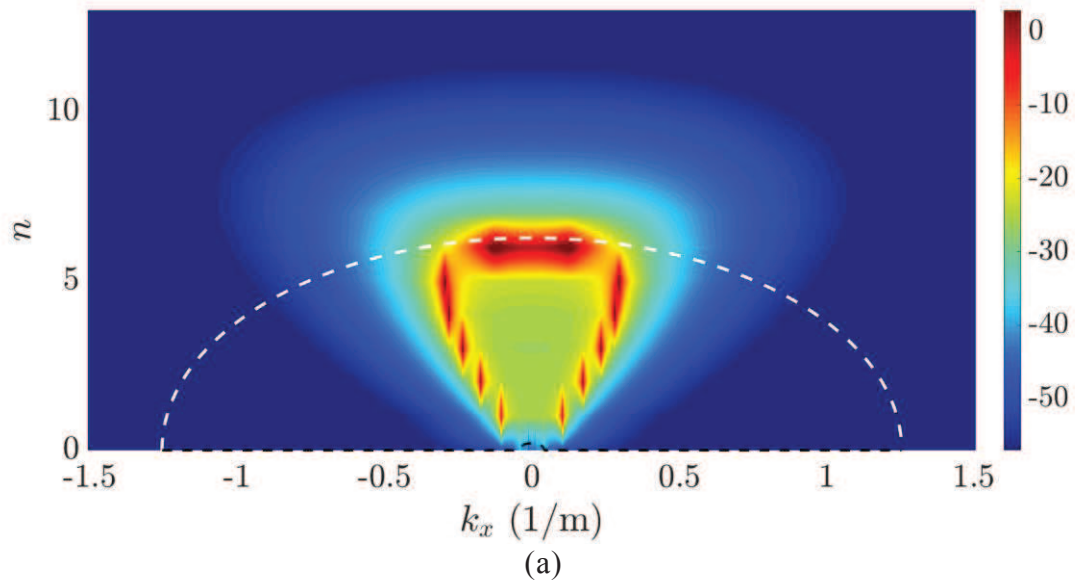
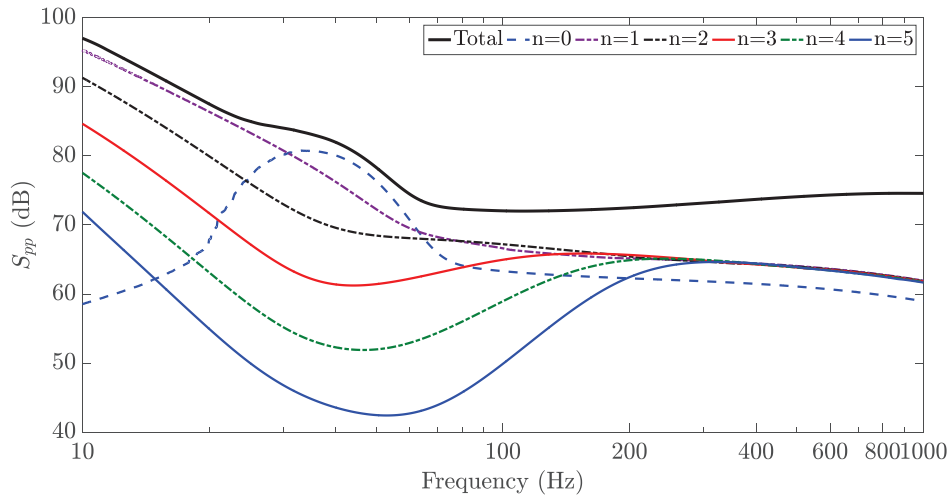


Fig 5. Circumferential sensitivity function in the acoustic near field ($z=0.1\text{m}$) at (a) 10 Hz, (b) 100 Hz and (c) 1000 Hz.

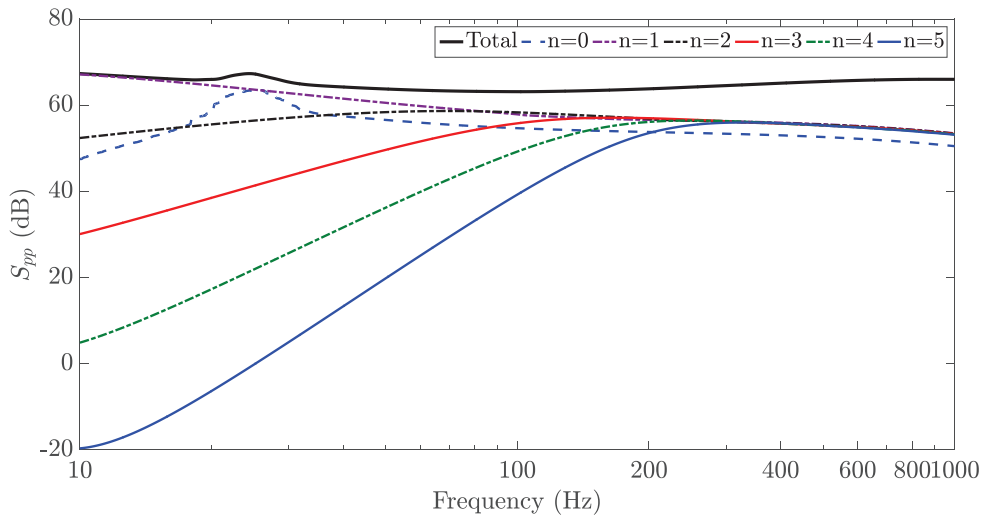
3.3 Far field acoustic spectra

The ASD function of the acoustic pressure and the corresponding circumferential sensitivity function are herein examined at increasing radial distances from the shell. Figure 6(a)-(c) presents the acoustic pressure as a function of frequency and including contributions by individual circumferential modes, at radial distances of $z=10$ m, $z=100$ m and $z=1000$ m, respectively. It can be observed that with increasing radial distance from the shell, the lowest order circumferential modes and in particular the $n=0$ mode, play an increasingly dominant role in the radiated pressure at low frequencies. This is attributed to the acoustic filtering effect associated with the blocked pressure \tilde{p}_b given by Eq. (12), and can be more clearly observed in the sensitivity function in Figure 7 (see also Williams et al. 1990). At very low frequencies, Figure 7 shows that only the lowest order modes occur within the supersonic wavenumber region with increasing distance from the shell, whereby all other wavenumber components are completely attenuated by the acoustic medium. Figure 8 shows that at a higher frequency (above the ring frequency), the same number of modes contribute to the acoustic spectrum for all three radial distances.

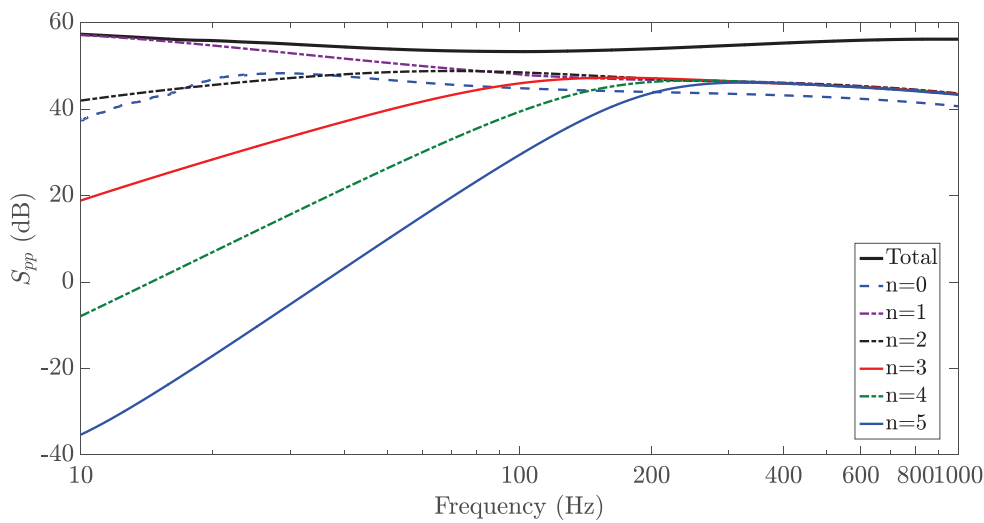
Figure 9 presents the ASD function of the radiated pressure at different radial distances from the shell surface. When the observation point is located in the near field ($z=0.1$ m and $z=1$ m), the pressure spectra exhibits a large number of fluctuations at low frequencies corresponding to the $n \geq 7$ modes for the frequency range considered here. When the receiver point is moved further away from the shell, the pressure spectrum becomes smoother and beyond a certain distance, remains almost constant with only slight variation within the frequency range of interest, associated with a similar number of modes contributing to the total spectrum as shown in Figure 8. In addition, the difference between spectrum levels becomes constant. An offset of approximately 10 dB between the spectrum levels at $z=10$ m, $z=100$ m and $z=1000$ m at higher frequencies can be observed, consistent with the $1/r$ decay law associated with cylindrical spreading (noting $r=R+z$).



(a)

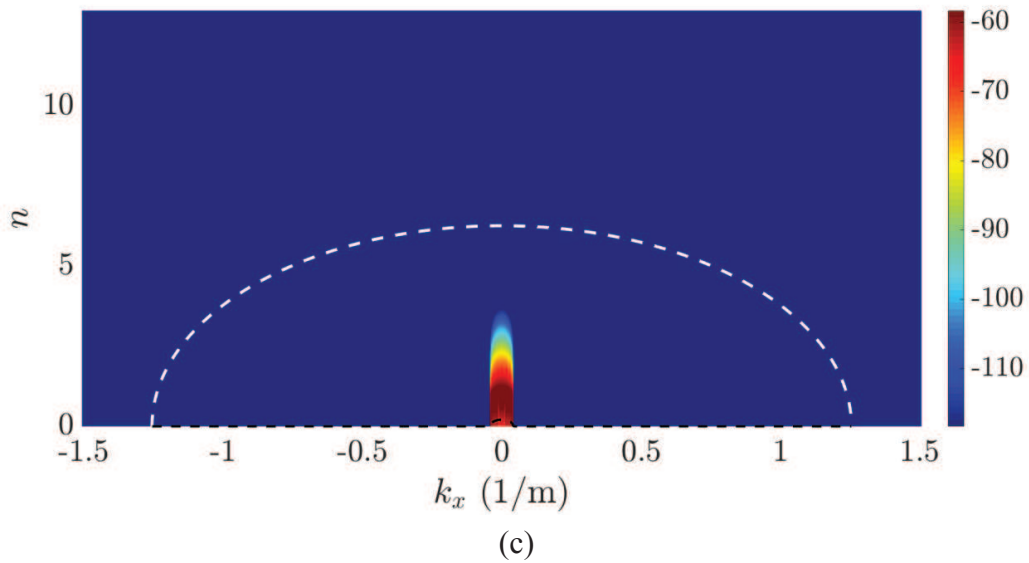
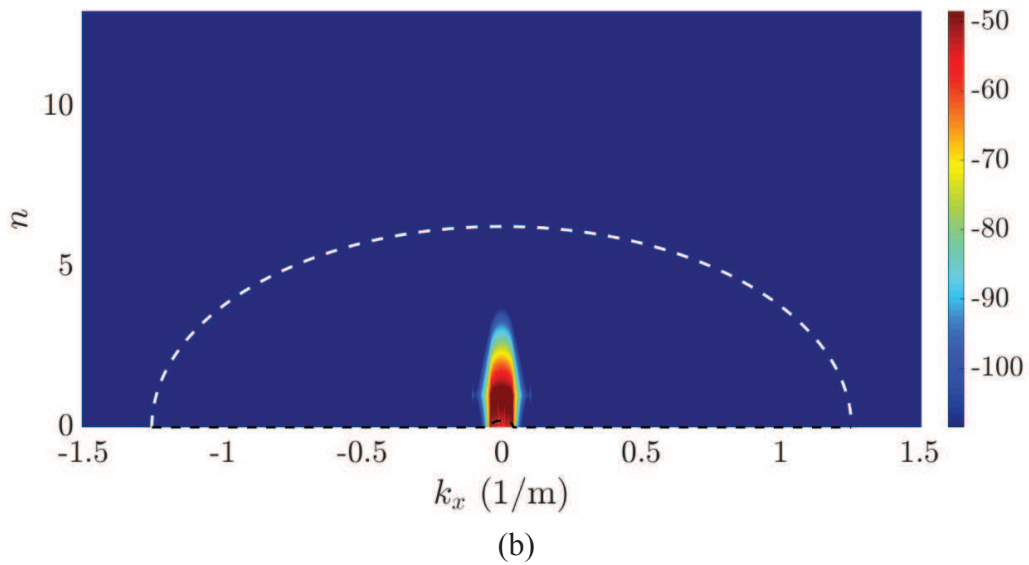
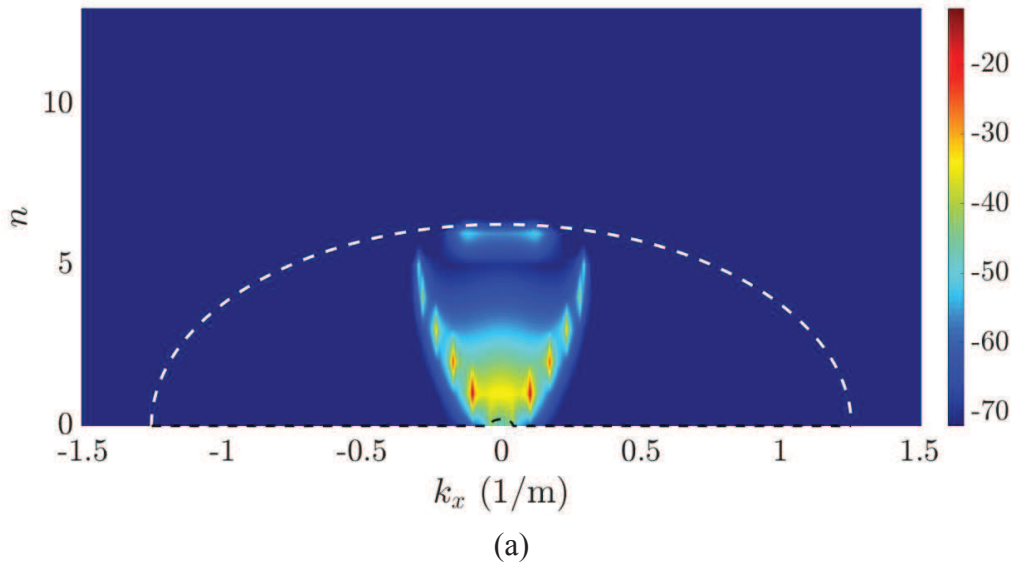


(b)



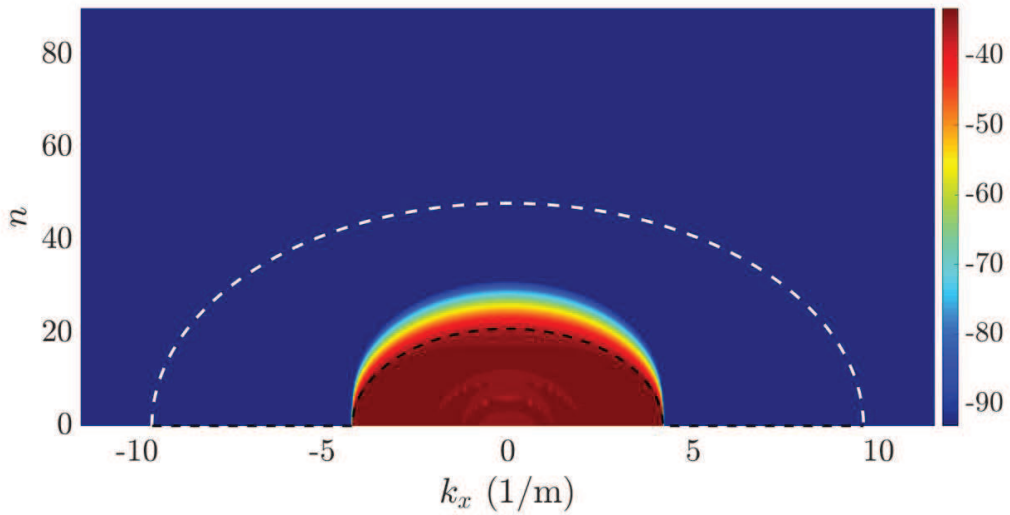
(c)

Figure 6. Auto spectral density of the acoustic pressure at (a) $z=10$ m, (b) $z=100$ m and (c) $z=1000$ m (dB ref. $1 \mu\text{Pa}/\sqrt{\text{Hz}}$).

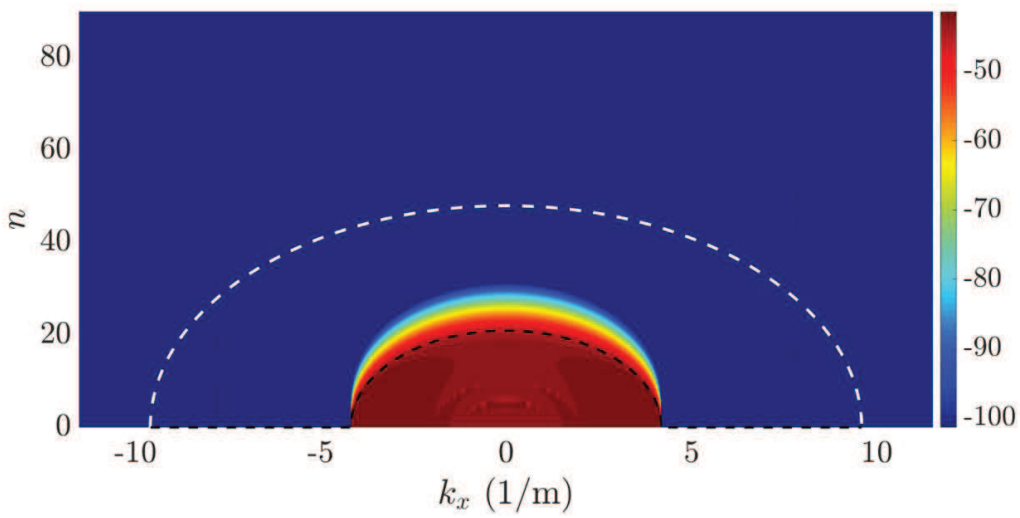


1350
1351
1352
1353
1354
1355
1356
1357

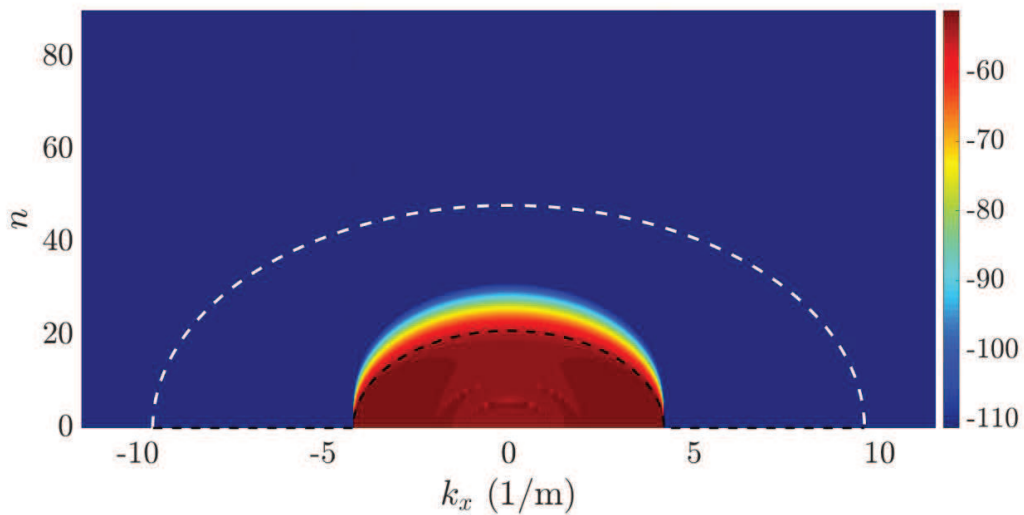
Figure 7. Circumferential sensitivity functions at a low frequency of 10 Hz at radial distances of (a) $z=10$ m, (b) $z=100$ m and (c) $z=1000$ m



(a) $z=10$ m



(b) $z=100$ m



(c) $z=1000$ m

Figure 8. Circumferential sensitivity functions at a high frequency of 1000 Hz at radial distances of (a) $z=10$ m, (b) $z=100$ m and (c) $z=1000$ m

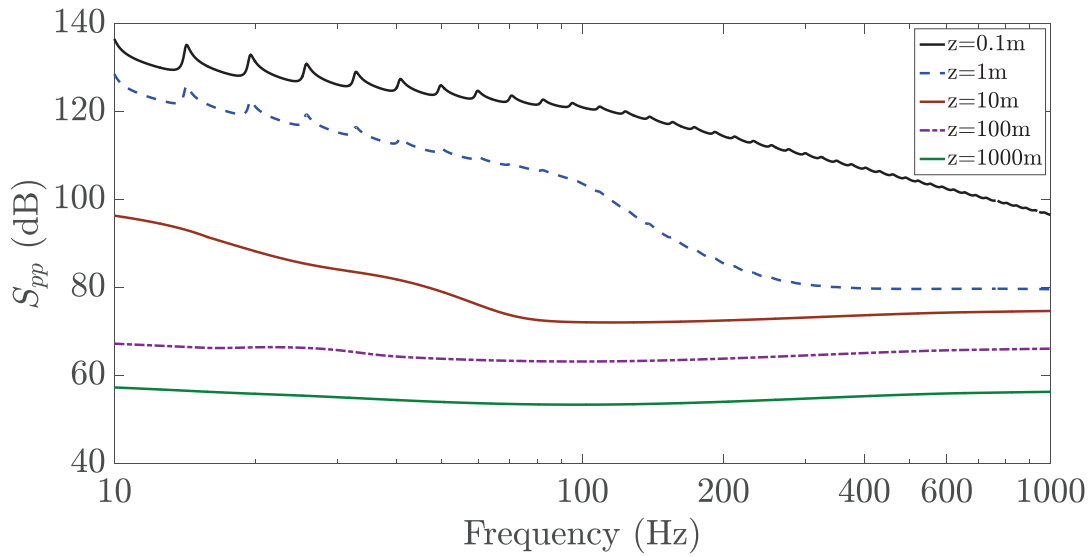


Figure 9. Auto spectral density of the acoustic pressure at different radial distances from the shell surface (dB ref. $1 \mu\text{Pa}/\sqrt{\text{Hz}}$)

3.4 Influence of the shell radius and flow speed

Figure 10 presents the radiated pressure spectra in the far-field ($z=1000 \text{ m}$) for different shell radii, showing a decrease in radiated pressure with an increase in shell radius. Figure 11 presents the pressure spectra at the three shell radii considered here and the corresponding contributions by individual circumferential modes. In Figure 10, the first two peaks for $R=0.5\text{m}$ occurring at 109 Hz and 321 Hz correspond to the $n=2$ and $n=3$ modes and the hump occurring approximately at 600 Hz corresponds to the $n=1$ circumferential mode, as shown in Figure 11(a). Similarly, the two visible peaks for $R=1\text{m}$ occurring at 24 Hz and 71 Hz correspond to the $n=2$ and $n=3$ modes, as shown in Figure 11(b). Figure 11 shows that the cut-on frequency of the shell circumferential modes for $n \geq 2$ decreases with increasing shell radius. The $n=0,1$ modes do not exhibit this cut-on effect (as discussed previously in Figure 4).

Figure 12 shows the effect of flow speed on the radiated sound in the far-field ($z=1000 \text{ m}$) for a cylindrical shell with a radius of $R=5 \text{ m}$. As shown in Table 1, three flow speeds were considered. The boundary layer thickness and friction velocity were assumed for

1476
 1477 flow speed of 6 m/s and a corresponding equivalent distance for TBL development on a
 1478 flat surface was estimated based on theoretical formula for a planar structure given by
 1479 Cengel and Cimbala (2006). The equivalent distance was then used for estimation of the
 1480 boundary layer thickness and friction velocity for flow speeds of 12 m/s and 24 m/s. These
 1481 TBL parameters were used in the Chase model to evaluate the CSD function of the WPF.
 1482 As expected, the radiated sound increases with an increase in the flow speed. Above 20
 1483 Hz, the radiated pressure increases by around 15 dB when the flow speed doubles from 6
 1484 m/s to 12 m/s, whereas it only increases by around 7 dB when the flow speed doubles from
 1485 12 m/s to 24 m/s. This is attributed to the significant increase in the friction velocity for a
 1486 flow speed from 6 m/s to 12 m/s, compared to its increase from 12 m/s to 24 m/s (see Table
 1487 1). The increase of the friction velocity leads to an increase of the ASD of the wall pressure
 1488 field induced by the TBL, which in turn leads to an increase of the radiated pressure.
 1489
 1490
 1491
 1492
 1493
 1494
 1495
 1496
 1497
 1498
 1499
 1500
 1501
 1502
 1503
 1504
 1505
 1506
 1507
 1508
 1509
 1510
 1511
 1512
 1513
 1514
 1515
 1516
 1517
 1518
 1519
 1520
 1521
 1522
 1523
 1524
 1525
 1526
 1527
 1528
 1529
 1530
 1531
 1532
 1533
 1534

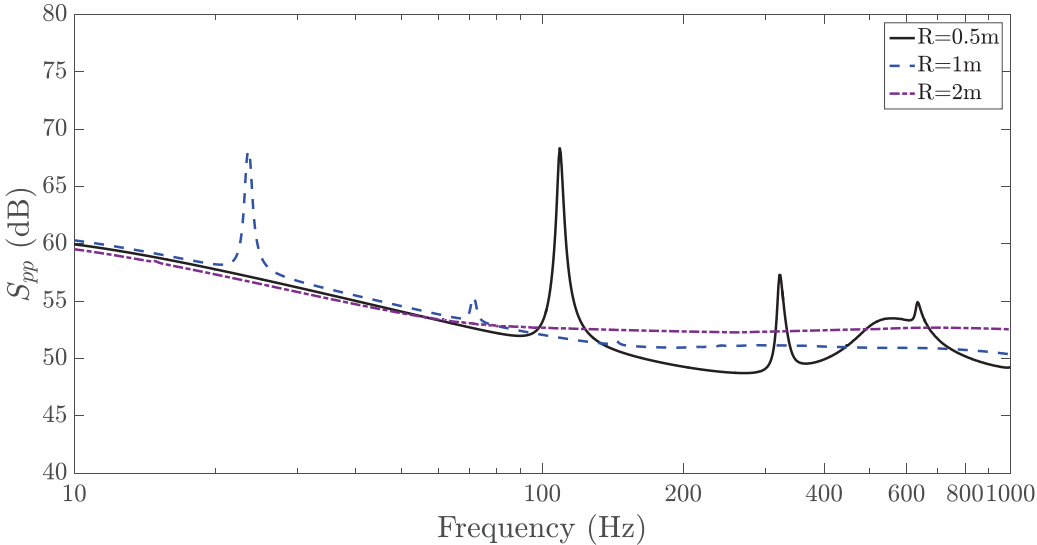
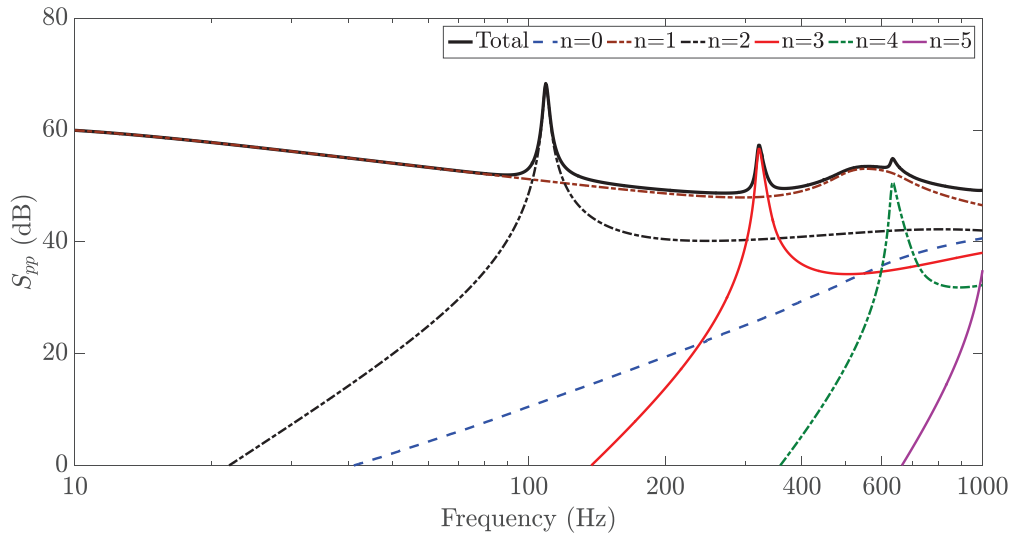
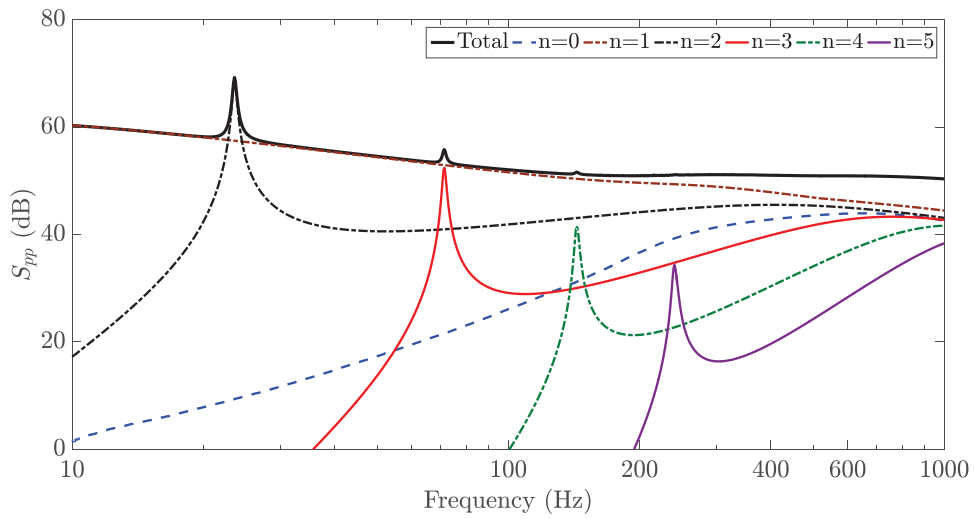


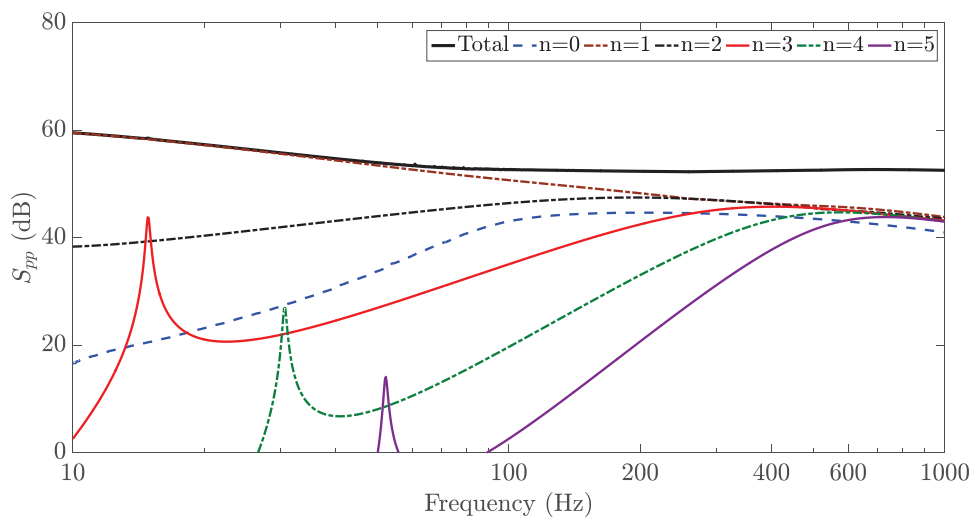
Figure 10. Auto spectral density of the acoustic pressure for different shell radii in the far field ($z=1000$ m)



(a)



(b)



(c)

Figure 11. Auto spectral density of the acoustic pressure for different shell radii in the far field ($z=1000$ m); (a) $R=0.5$ m, (b) $R=1$ m, (c) $R=2$ m, (dB ref. $1 \mu\text{Pa}/\sqrt{\text{Hz}}$).

Table 1. Boundary layer parameters used to compute the ASD in Figure 12

Free stream velocity	Boundary layer thickness	Friction velocity
U_{∞} (m/s)	δ (m)	v_{τ} (m/s)
6	0.15	1
12	0.13	1.87
24	0.11	2.26

Figure 13 presents the simulation run time to compute the radiated sound using the present approach as a function of frequency for the cylinder with a radius of $R=5$ m. Simulations were conducted using MATLAB on a desktop personal computer with 32 GB of random access memory (RAM) and a total of four physical cores running at 3.2 GHz. It can be seen from Figure 13 that as the frequency increases, the computational time increases dramatically. This is attributed to the fact that more wavenumbers and circumferential modes need to be considered in the computation at high frequencies. A linear function corresponding to $0.0039f - 0.0324$ was curve fitted to the simulation run time data and is also shown in Figure 13, clearly highlighting that the run time varies linearly with frequency. For the cylindrical shell model considered here, the maximum run time for the highest frequency of interest at 1 kHz is less than 4 seconds.

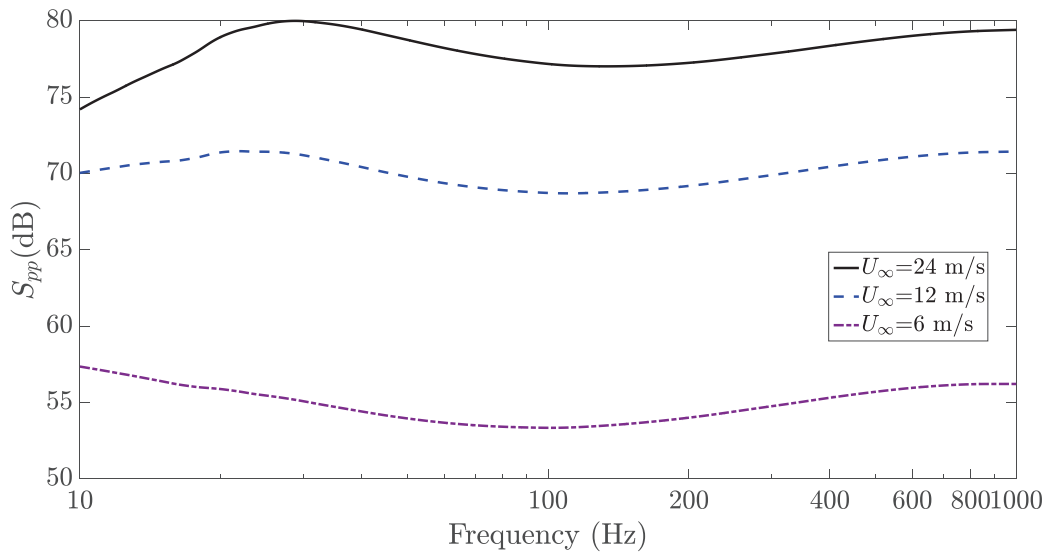


Figure 12. Auto spectral density of the acoustic pressure in the far field ($z=1000$ m) for different flow speeds.

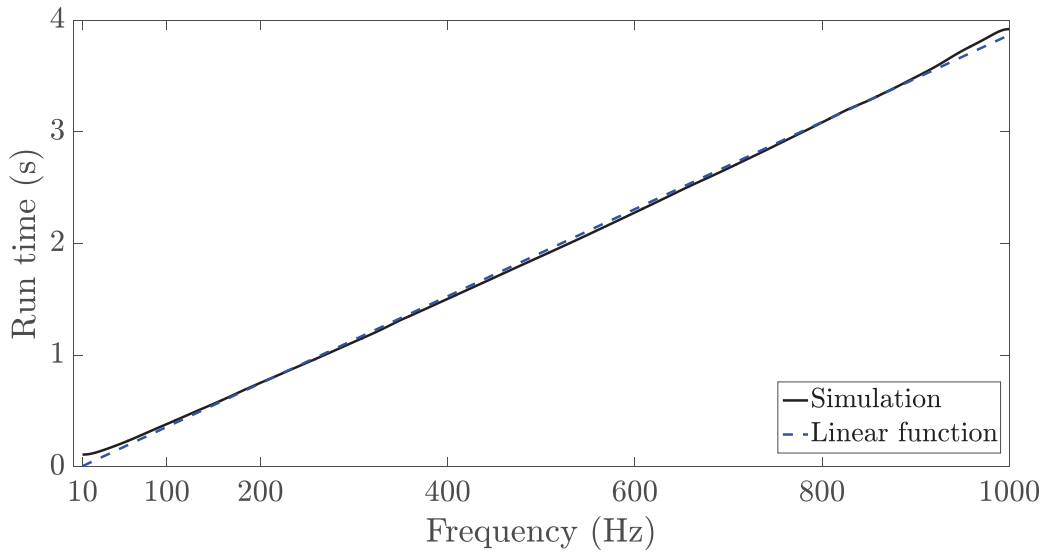


Figure 13. Computational run time to compute the radiated acoustic pressure

4. Summary

An analytical model of a fluid loaded cylindrical shell excited by a turbulent flow field has been presented. A wavenumber-point reciprocity principle was implemented to identify circumferential sensitivity functions. The Chase model was used to describe the wall pressure field induced by the turbulent boundary layer in the wavenumber-frequency domain. Our proposed method provides the ability to investigate the physical mechanisms associated with the noise radiated by a cylindrical shell excited by a TBL, by examining the contributions by individual circumferential modes to the acoustic spectra. The pressure spectra in both in the near field and far field were presented for frequencies below and above the ring frequency, as well as for different shell radii and flow speeds. The proposed method is also an efficient computational tool for evaluation of the vibroacoustic responses of a cylindrical shell under flow excitation, typically found in maritime applications. In the near future, we will implement our numerical approach to study more realistic designs of a submerged marine vessel that incorporate the effects of ring stiffeners and other internal structures of the hull.

Acknowledgement

This work was carried out in the framework of the LabEx CeLyA (“Centre Lyonnais d'Acoustique”, ANR-10-LABX-60). The second author gratefully acknowledges financial support from the Australian Government through the Australian Research Council’s Discovery Projects funding scheme (project DE190101412).

Appendix A

The elements of the spectral Flügge operator $\mathcal{L}(x, \theta)$ are given by (Karczuz, 2006)

$$\mathcal{L}(x, \theta) = \begin{Bmatrix} Z_{UU} & Z_{UV} & Z_{UW} \\ Z_{UV} & Z_{VV} & Z_{VW} \\ Z_{UW} & Z_{VW} & Z_{WW} \end{Bmatrix}, \quad (\text{A1})$$

$$Z_{UU} = R^2 \frac{\partial^2}{\partial x^2} - \rho_s R^2 \frac{1-\nu^2}{E} \frac{\partial^2}{\partial t^2} + (1+\beta^2) \frac{1-\nu}{2} \frac{\partial^2}{\partial \theta^2}, \quad (\text{A2})$$

$$Z_{UV} = R \frac{1+\nu}{2} \frac{\partial^2}{\partial x \partial \theta}, \quad (\text{A3})$$

$$Z_{UW} = R\nu \frac{\partial}{\partial x} - \beta^2 R^3 \frac{\partial^3}{\partial x^3} + \beta^2 R \frac{1-\nu}{2} \frac{\partial^3}{\partial x \partial \theta^2}, \quad (\text{A4})$$

$$Z_{VV} = (1+3\beta^2) R^2 \frac{1-\nu}{2} \frac{\partial^2}{\partial x^2} + \frac{\partial^2}{\partial \theta^2} - \rho_s R^2 \frac{1-\nu^2}{E} \frac{\partial^2}{\partial t^2}, \quad (\text{A5})$$

$$Z_{VW} = \frac{\partial}{\partial \theta} - \beta^2 R^2 \frac{3-\nu}{2} \frac{\partial^3}{\partial x^2 \partial \theta}, \quad (\text{A6})$$

$$Z_{WW} = 1 + \beta^2 \left(R^4 \frac{\partial^4}{\partial x^4} + 2R^2 \frac{\partial^4}{\partial x^2 \partial \theta^2} + \frac{\partial^4}{\partial \theta^4} \right) + \rho_s R^2 \frac{1-\nu^2}{E} \frac{\partial^2}{\partial t^2} + \beta^2 \left(1 + 2 \frac{\partial^2}{\partial \theta^2} \right), \quad (\text{A7})$$

where $\beta = \frac{h}{\sqrt{12}R}$ is the shell thickness parameter.

Appendix B

The elements of the spectral Flügge operator $\tilde{\mathcal{L}}(k_x, n)$ in the wavenumber domain are given

by

$$\tilde{\mathcal{L}}(k_x, n) = \begin{bmatrix} \tilde{Z}_{UU} & \tilde{Z}_{UV} & \tilde{Z}_{UW} \\ \tilde{Z}_{UV} & \tilde{Z}_{VV} & \tilde{Z}_{VW} \\ \tilde{Z}_{UW} & \tilde{Z}_{VW} & \tilde{Z}_{WW} \end{bmatrix}, \quad (\text{B1})$$

$$\tilde{Z}_{UU} = R^2(k_l^2 - k_x^2) - n^2 \frac{1-\nu}{2}(1 + \beta^2), \quad (\text{B2})$$

$$\tilde{Z}_{UV} = -nR \frac{1+\nu}{2} k_x, \quad (\text{B3})$$

$$\tilde{Z}_{UW} = ik_x \left(R\nu - \beta^2 \left(-R^3 k_x^2 + n^2 R \frac{1-\nu}{2} \right) \right), \quad (\text{B4})$$

$$\tilde{Z}_{VV} = -R^2 \frac{1-\nu}{2} k_x^2 (1 + 3\beta^2) - n^2 + R^2 k_l^2, \quad (\text{B5})$$

$$\tilde{Z}_{VW} = in \left(1 + \beta^2 R^2 \frac{3-\nu}{2} k_x^2 \right), \quad (\text{B6})$$

$$\tilde{Z}_{WW} = 1 + \beta^2 \left(R^4 k_x^4 + 2n^2 (R^2 k_x^2 + 1) + n^4 + 1 \right) - R^2 k_l^2, \quad (\text{B7})$$

where $k_l = \omega \sqrt{\frac{\rho_s(1-\nu^2)}{E}}$ is the wavenumber for longitudinal waves propagating in the

cylindrical shell.

Appendix C

The cross spectral density of the Chase TBL model for a planar structure is given by (Chase, 1987)

$$\varphi_{pp}(k_x, k_y, \omega) = \frac{(2\pi)^3 \rho_f^2 v_\tau^3}{(K_+^2 + (b\delta)^{-2})^{5/2}} \left(C_M k_x^2 + C_T K^2 \left(\frac{K_+^2 + (b\delta)^{-2}}{K^2 + (b\delta)^{-2}} \right) \right) \quad (C1)$$

with $K_+^2 = (\omega - U_c k_x)^2 / (qv_\tau)^2 + K^2$ and $K^2 = k_x^2 + k_y^2$. Recommended parameters for $b, q,$

C_M, C_T are given as $b=0.75, q=3, C_M \approx 0.1553$ and $C_T \approx 0.0047$ (Howe, 1998).

REFERENCES

Chase, D.M., 1987. The character of the turbulent wall pressure spectrum at subconvective wavenumbers and a suggested comprehensive model. *J. Sound Vib.* 112(1), 125-147.

Cengel, Y., Cimbala, J., 2006. *Fluid Mechanics: Fundamentals and Applications*. McGraw-Hill series in mechanical engineering, Mc Graw-Hill Higher Education.

Ciappi, E., De Rosa, S., Franco, F., Guyader, J.L., Hambric, S.A., 2014. *Flinovia-flow induced noise and vibration issues and aspects*, Springer International Publishing Switzerland.

Ciappi, E., De Rosa, S., Franco, F., Guyader, J.L., Hambric, S.A., Leung, R.C.K. and Hanford, A.D., 2018. *Flinovia-Flow Induced Noise and Vibration Issues and Aspects-II*. Springer International Publishing Switzerland.

Ciappi, E., Magionesi, F., De Rosa, S. and Franco, F., 2009. Hydrodynamic and hydroelastic analyses of a plate excited by the turbulent boundary layer. *J. Fluids Struct.*, 25(2), 321-342.

Ciappi, E., De Rosa, S., Franco, F., Vitiello, P. and Miozzi, M., 2016. On the dynamic behavior of composite panels under turbulent boundary layer excitations. *J. Sound Vib.* 364, 77-109.

Corcus, G. M., 1963. Resolution of pressure in Turbulence, *J. Acoust. Soc. Am.* 35, 192-199.

Crocker, M.J., 1998. *Handbook of acoustics*. John Wiley & Sons.

1948
1949
1950
1951
1952
1953
1954
1955
1956
1957
1958
1959
1960
1961
1962
1963
1964
1965
1966
1967
1968
1969
1970
1971
1972
1973
1974
1975
1976
1977
1978
1979
1980
1981
1982
1983
1984
1985
1986
1987
1988
1989
1990
1991
1992
1993
1994
1995
1996
1997
1998
1999
2000
2001
2002
2003
2004
2005
2006

Davis, H. G., 1971. Sound from turbulent boundary layer excited panel, *J. Acoust. Soc. Am.* 49, 878-889.

De Rosa, S. and Franco, F., 2008. Exact and numerical responses of a plate under a turbulent boundary layer excitation. *J. Fluids Struct.* 24(2), 212-230.

Durant, C., Robert, G., Filippi, P.J.T., Mattei, P.O., 2000. Vibroacoustic response of a thin cylindrical shell excited by a turbulent internal flow: comparison between numerical prediction and experimentation. *J. Sound Vib.* 229(5), 1115-1155.

Errico, F., Ichchou, M., Franco, F., De Rosa, S., Bareille, O. and Droz, C., 2019. Schemes for the sound transmission of flat, curved and axisymmetric structures excited by aerodynamic and acoustic sources. *J. Sound Vib.* 456 (15), 221-238.

Fahy, F.J. and Gardonio, P., 2006. *Sound and structural vibration: Radiation, transmission and response.* Academic Press.

Goody, M. C., 2004. Empirical spectral model of surface pressure fluctuations, *AIAA J.*, 42, 1788-1794.

Hambric, S.A., Hwang, Y.F. and Bonness, W.K., 2004. Vibrations of plates with clamped and free edges excited by low-speed turbulent boundary layer flow. *J. Fluid Struct.* 19(1), 93-110.

Howe, M.S., 1998. *Acoustics of fluid-structure interactions.* Cambridge University Press.

James, J.H., 1982. *Computation of Acoustic Power, Vibration Response and Acoustic pressures of fluid-filled pipes.* Admiralty marine technology establishment Teddington (England). no. 82036.

Junger, M.C. and Feit, D., 1986. *Sound, structures, and their interaction,* Cambridge, MA: MIT press.

Karczub, D.G., 2006. Expressions for direct evaluation of wave number in cylindrical shell vibration studies using the Flügge equations of motion. *J. Acoust. Soc. Am.* 119(6), 3553-3557.

Leissa, A.W., 1973. *Vibration of shells.* Washington: Scientific and Technical Information Office, National Aeronautics and Space Administration.

- 2007
2008
2009
2010
2011
2012
2013
2014
2015
2016
2017
2018
2019
2020
2021
2022
2023
2024
2025
2026
2027
2028
2029
2030
2031
2032
2033
2034
2035
2036
2037
2038
2039
2040
2041
2042
2043
2044
2045
2046
2047
2048
2049
2050
2051
2052
2053
2054
2055
2056
2057
2058
2059
2060
2061
2062
2063
2064
2065
- Li, Y., Zhang, Y. and Kennedy, D., 2017. Random vibration analysis of axially compressed cylindrical shells under turbulent boundary layer in a symplectic system. *J. Sound Vib.* 406, 161-180.
- Liu, B., 2008. Noise radiation of aircraft panels subjected to boundary layer pressure fluctuations. *J. Sound Vib.* 314, 693-711.
- Lueptow, R.M., 1988. Turbulent boundary layer on a cylinder in axial flow, Technical report, DTIC Document.
- Maxit, L. and Ginoux, J.M., 2010. Prediction of the vibro-acoustic behavior of a submerged shell non periodically stiffened by internal frames. *J. Acoust. Soc. Am.* 128(1), 137-151.
- Marchetto, C., Maxit, L., Robin, O. and Berry, A., 2017. Vibroacoustic response of panels under diffuse acoustic field excitation from sensitivity functions and reciprocity principles. *J. Acoust. Soc. Am.* 141(6), 4508-4521.
- Marchetto, C., Maxit, L., Robin, O. and Berry, A., 2018. Experimental prediction of the vibration response of panels under a turbulent boundary layer excitation from sensitivity functions. *J. Acoust. Soc. Am.* 143(5), 2954-2964.
- Maxit, L. and Denis, V., 2013. Prediction of flow induced sound and vibration of periodically stiffened plates. *J. Acoust. Soc. Am.* 133(1), 146-160.
- Maxit, L., 2016. Simulation of the pressure field beneath a turbulent boundary layer using realizations of uncorrelated wall plane waves, *J. Acoust. Soc. Am.* 140, 1268-1285.
- Maury, C., Gardonio, P. and Elliott, S.J., 2002a. A wavenumber approach to modelling the response of a randomly excited panel, part I: general theory. *J. Sound Vib.* 252(1), 83-113.
- Maury, C., Gardonio, P. and Elliott, S.J., 2002b. A wavenumber approach to modelling the response of a randomly excited panel, Part II: Application to aircraft panels excited by a turbulent boundary layer. *J. Sound Vib.* 252(1), 115-139.
- Mazzoni, D., 2003. An efficient approximation for the vibroacoustic response of a turbulent boundary layer excited panel, *J. Sound Vib.* 264, 951-971.
- Norton, M.P. and Bull, M.K., 1984. Mechanisms of the generation of external acoustic radiation from pipes due to internal flow disturbances. *J. Sound Vib.* 94(1), 105-146.

2066
2067 Photiadis, D.M., 1990. The propagation of axisymmetric waves on a fluid-loaded cylindrical
2068 shell, J. Acoust. Soc. Am. 88, 239-250.
2069

2070
2071 Strawderman, W.A., 1969. Turbulence-induced plate vibrations: An evaluation of finite- and
2072 infinite-plate models, J. Acoust. Soc. Am. 46, 1294-1295.
2073

2074
2075 Strawderman, W.A., Christman, R.A., 1971. Turbulence-induced plate vibrations: Some
2076 effects of fluid loading on finite and infinite plates, J. Acoust. Soc. Am. 52, 1537–1552.
2077

2078
2079 Scott, J.F.M., 1988. The free modes of propagation of an infinite fluid-loaded thin cylindrical
2080 shell. J. Sound Vib. 125(2), 241-280.
2081

2082
2083 Tang, Y., Silcox, R., Robinson, J., 1996. Sound transmission through cylindrical shell
2084 structures excited by boundary layer pressure fluctuations. In Aeroacoust. Conf. p. 1760.
2085

2086
2087 Williams, E.G., Houston, B.H., Bucaro, J.A., 1990. Experimental investigation of the wave
2088 propagation on a point-driven, submerged capped cylinder using *K*-space analysis, J. Acoust.
2089 Soc. Am. 87, 513–552.
2090

2091
2092 Williams, E.G., 1999. Fourier acoustics: sound radiation and nearfield acoustical holography.
2093 Academic press, Elsevier.
2094

2095
2096 Zhang, Q., Mao, Y. and Qi, D., 2018. Analytical modeling of the vibro-acoustic response of a
2097 double-walled cylindrical shell with microperforation excited by turbulent boundary layer
2098 pressure fluctuations. J. Vib. Acoust, 140(2), 1-13.
2099

2100
2101 Zhou, J., Bhaskar, A. and Zhang, X., 2015. Sound transmission through double cylindrical
2102 shells lined with porous material under turbulent boundary layer excitation. J. Sound Vib. 357,
2103 253-268.
2104
2105
2106
2107
2108
2109
2110
2111
2112
2113
2114
2115
2116
2117
2118
2119
2120
2121
2122
2123
2124